JCHR (2025) 15(2), 283-297

Journal of Chemical Health Risks

sanad.iau.ir/journal/jchr

ORIGINAL ARTICLE

Novel Nitrogen-Doped Carbon Dots for Degrading Azo Dyes and Sensing Heavy Metals

Mohd Abdullah sheikh[*1], Ravinder Singh Chandok [2], Khan Abida[3]

[1]*Research Scholar Bhagwant University,* Ajmer-305004 Rajasthan, *India*

[2]*Sri Guru Tegh Bahadur Khalsa College (Jabalpur), India*

[3]*Shaheed Himayun Muzzamil Memorial, Government Degree College, Anantnag (J & K), India*

(Received: 12 January 2024 Accepted: 3 July 2024)

KEYWORDS

N-CDs;
Pumpkin seeds;
Microwave irradiation;
Urea;
Mercury;
Congo-red;
TiO_2/N-CDs

ABSTRACT: This work presents an application perspective of recently developed, novel green synthesized self-heteroatom doped N-carbon dots (N-CDs) derived from biomass pumpkin seeds, possessing an energy gap of 2.35 eV and an unremarkable quantum efficiency of 65.5%, besides a graphitic carbon structure they are doped with various metal and nonmetal ions and an overall size distribution of 5-8 nm. Here we have used them as a novel photocatalyst by mixing them with widely known photocatalyst titanium dioxide, thereby enhancing the overall photocatalytic efficiency of the amalgam of both materials. Further, this novel amalgam of Carbon dots has demonstrated a well-distinguished FTIR, XRD, and UV absorbance and emission wavelength spectra, and displayed a broad absorbance wavelength spectra in lower energy region, hence more efficient compared to pure Titanium dioxide. Thus the composite of TiO_2/N-CDs degraded Congo red dye in a short duration of 18 minutes, illuminated under UV light, and has shown 90% degradation efficiency. However, only 40% degradation was shown by pure N-CDs. Further, we have used these Carbon dots as a sensing material for the detection of heavy metal ions and the results have demonstrated a good detection limit of the heavy metal Hg^{2+} ions among other tested metal ions, owing to its excellent selective and sensitive property of fluorescent quenching analysis, resulted in the creation of non-fluorescent centers, effective charge transfer and overall energy transfer, with a minimum detection threshold limit of 20 nM.

INTRODUCTION

Carbon dots, also known as CDs, are a significant component of carbon-based nanomaterials which adjusts its size from 1 to 10 nm. They were initially identified in 2004 as quantum dots, and they were recently awarded the Noble Prize 2023 for their discovery and fabrication. The preparation mainly involves the process of pyrolysis, of carbon-based biotic and abiotic components, resulting in the breakdown, hydrolysis, and carbonization of the precursor content thereby, undergo significant changes in their physical and chemical properties, with a high quantum yield and a regulated emission wavelength [1–10]. These carbon dots have exposed novel areas of usage due to their effective stability towards light, lower cytotoxicity risk, superior host compatibility, ease of surface modification, and inert chemical behavior in the creation of fluorescent sensors, energy reservoirs, active cell imaging, in vivo research, photocatalytic degradation, and colored (LEDs) [11–21].

Presently, researchers focus on green preparation of nanomaterials and lot of work has been done to produce

*Corresponding author: absheikh1989@gmail.com (M. Abdullah sheikh)
DOI: 10.60829/JCHR.2024.1121944

these nanomaterials from numerous biomass resources, including lychee seed (10.3%) [22], dairy milk (12%) [23], strawberry juice (6.3%) [24], soy milk (2.6%), [25] and (QY for the generated CDs is provided in parenthesis), have been used as precursors in the hydrothermal synthesis of N-CDs. Through doping carbon nanostructure with heteroatoms such as N, B, P, S, and so on, scientists have improved carbonaceous materials' electro-catalytic properties. Research has shown that doping carbon nanomaterials such as graphene, carbon nanotubes, and graphene-coated diamonds (GCDS), with different heteroatoms, has demonstrated several benefits over non-doped carbon nanomaterials. Firstly, the introduction of heteroatoms into the carbon network and the presence of redox-active sites allowed for the addition of electro-catalytic active sites with only minor modifications to the conjugation length [26]. The domains of hazardous heavy metal ion sensing and electrocatalytic gas sensing are very interested in these advantageous properties [27].

Presently, the environment is on the verge of degradation and requires collective efforts through sustained practices and practical measures. Among all these pollutants, presiding in the environment, one of the most harmful and pervasive contaminants in the environment is the mercury (II) ion (Hg^{2+}), which is classified among the highly poisonous heavy metal ions [28]. It is contaminated by several different natural processes as well as human activity [29]. Nearly 4,400–7,500 metric tons of mercuryis estimated to be discharged annually by the UNEP [30]. Hg^{2+} may readily enter the body through the skin, respiratory, and gastrointestinal tissues and damage the central nervous system and endocrine system, which makes it a major hazard to human health [31]. Hence, much effort has been paid to the advancement of effective analytical methods for the precise and sensitive measurement of $Hg^{2+.}$ The methods now used to detect Hg^{2+} include polarography, inductively coupled plasma mass spectrometry, atomic fluorescence spectrometry, and atomic absorption/emission spectroscopy [32].These element-specific detectors, are typically paired with complex instrumentation, are time-consuming, expensive, and unsuitable for real-world applications. Fluorescence assays can be used as an alternative to optical sensing techniques in the detection of Hg^{2+} due to their high sensitivity, quick analysis, and non-sample destruction or little cell harm. Presently, a wide variety of fluorescent probes, such as organic molecules, metal nano-clusters, and semiconductor quantum dots, are available for fluorescent sensing of Hg^{2+} detection [33-34]. These fluorescent compounds, however, encounter difficult synthesis techniques or the consumption of hazardous or costly chemicals. Therefore, it is highly desired to create easy, inexpensive, and environmentally friendly preparative methods for fluorescent materials.

Besides that, several toxic materials prevalent in drinking water which is used by textile industries and medical laboratories as color stains are organic toxic dyes. Therefore it is the need of the hour to safely degrade these dyes, prevalent in real water samples to assure the quality of life. Research is going on against the removal of these harmful substances that have focused primarily on the use of metal oxide nanomaterials [35-38]. However, the use of these metal oxides has worsened environmental conditions because they have been used in critical environmental conditions and resulted in the use of toxic chemicals which have permanently settled in the environment and require further action. Therefore, to replace those hazardous chemicals, a unique green photocatalyst is required. Because TiO_2 nanoparticles are low in toxicity, chemically inert, highly efficient, and inexpensive, they have been investigated for their potential photocatalytic activities in the photocatalytic destruction of hazardous dyes [39–40]. A few drawbacks of TiO_2 include quick electron-hole recombination, a broad, short UV band gap energy, high concentration aggregation, and a deficiency of specific surface area, which restrict its effectiveness in photodegradation. The addition of carbonaceous elements to TiO_2 surfaces has been proposed as a solution to these problems. Transferring photoexcited electrons from TiO_2 to these materials would enable them to function as binding sites for electron-hole couples, perhaps halting the rapid electron and hole recombination, thereby boosting TiO2's photocatalytic efficiency [41–44]. The development of CQD/TiO_2nanocomposite material with increased photocatalytic activity for the breakdown of organic contaminants has been the subject of several investigations [45]. Additionally, the specific surface

area and electrical properties of CQDs have significantly increased by doping them with light heteroatoms (B, N, P, and S) thereby, boosting their photocatalytic activity and all other basic features [46-55]. As a result, it has been anticipated that heteroatom-doped CDs could improve TiO_2's capacity of photo-catalysis and long-term stability towards elimination of those hazardous substances.

Nitrogen, spontaneous trace elements like phosphorus, sulfur, zinc, potassium, and magnesium were incorporated into green synthesized blue emitting Nitrogen-Carbon dots, written as N-CDs, have a size distribution ranging from 5 to 8 nm, with a broad absorption band located between 250 and 550 nm and a notable fluorescence region observed between 400 and 600 nm. With an overall quantum yield of 65.50 percent, the fluorescence emission spectra displayed typical excitation-dependent behavior [56]. They have displayed the effective quenched fluorescence-based sensing of Hg^{2+} metal ions. The results have demonstrated that the reaction of Hg^{2+} metal ions with the N-CDs dispersed in the phosphate buffer sol at PH-7 showed a 50% fluorescence quenching within only 10 minutes of solution mixing, with a detection limit of 20nM. Therefore, self-heteroatom doped N-CQDs have been effectively utilized for examiningHg^{2+} ions in actual water samples.

Another important application associated with environmental sustainability is the photodegradation of toxic dyes, therefore under short UV light, a composite made of N-CQDs and TiO_2 showed a high degree of photocatalytic activity in the breakdown of Congo red azo dye. When compared to carbon dots which act as an independent photocatalyst, have demonstrated almost 40% degrading efficiency at the same concentration and exposure time. In contrast, a combination of N-CQDs and TiO_2 demonstrated a 90% overall photocatalytic efficiency when it came to breaking down Congo red. This photodegradation was primarily brought about by the formation of ROS in the solvent system as a result of the composite's multiple active sites and defects, which caused oxygen species to adsorb and reduce onto the surface and prevented electrons and holes from recombining within the composite. As a result, electrons were effectively transferred from N-CDs to TiO_2 and vice-versa.

MATERIALS AND METHODS

Materials and chemicals

Pure TiO_2 powder, NF, HCL, H_2SO_4, Carbon black, PVDF, ethanol, $Zn(OAc)_2$, $Pb(NO_3)_2$, $NiCl_2$, $Hg(NO_3)_2$, $CaCl_2$, $CuCl_2$, $Mg(OAc)_2$, phosphate buffer (PH 7.0), iodide solution purchased from local market and Congo red azo dye from local market, all the materials and chemicals are 99% pure and of laboratory grade.

Methodology and synthesis

The synthesis of spontaneous heteroatom doped N-carbon dots was recently reported by our team Abdullah et al. [56], utilizing urea as a nitrogen source for surface passivation and pumpkin seeds as the carbon source at a weight percent ratio of 1:1. A dark, solid residue was seen when the slurry was subjected to 900 watts of microwave radiation for eight minutes. Larger, untreated particles were then eliminated from the solution by passing it through a 0.21-micron syringe filter. In the end, remove the ions and small molecules by using a 10000 MWCO dialysis membrane for six hours, and finally the pH was adjusted to around 5 by adding NaOH to the solution, then, dried at 60 degrees for 2 days to obtain a fine powder of N-CDTs.

Preparation of working electrode for CV measurements

The produced hetero-atom doped N-CDs were combined with carbon black and a binder (PVDF) at W% values of 90, 5, and 5. After that, the mixture was combined with 5 mL of ethanol and distilled water. The mixture was stirred for a short while before being sonicated for 30 minutes at 40 kHz to produce a well-dispersed precipitate. The nickel foam was immersed in a diluted 2M HCLsolution to remove impurities and stains, and then it was thoroughly washed with DI water. Carefully applying the slurry on the NF, it was allowed to dry for fifteen minutes before being sintered for thirty minutes at 80°C. The final working electrode was created with a loading of 1 $mgcm^{-2}$ of working material, and it was then kept in storage awaiting additional processing.

Preparing different concentrations of N-CDs and metal ion solutions

1 mL of phosphate buffer (0.05M) was immersed in 10 µL of diluted photoluminescent heteroatom doped N-CDs solution and 0.005, 0.010, 0.020, 0.030, and 0.050 µM's of Hg^{2+}were pipetted into a 2 mL vial simultaneously. The mixture was then diluted to 250 µL with water and thoroughly mixed. In the same way, the other metal ion buffer solutions were produced with an optimal concentration of (0.020 µM) with these N-CDs. The photoluminescence emission spectra were recorded after 10 min of reaction time at room temperature. Similarly, prepare a dispersion of Hg^{2+} ionic solution in buffer with tap water, spring water, and river water after centrifuging at 5000 rpm for 10 minutes and filtered the water samples by 0.22 µm syringe filters.

Preparation of modified self-heteroatom doped N-CDs/TiO_2hybrid Photo-catalyst

The first step included dispersing 1 g of TiO_2 powder and 1 g of synthesized N-carbon dots with 30 ml of DI. Subsequently, the mixture was ultrasonically processed in an ultrasonic bath for 30 minutes and irradiated with a frequency of 40 kHz to produce a well-dispersed suspension. After being transferred to a glass beaker, this solution was micro-waved for five minutes at 900 W to get the required photocatalyst. Following centrifugation at 5000 rpm, the final product was cleaned three or four times using DI water and ethanol and then dried for twenty-four hours at 70 ℃ in an oven. Then, the photocatalyst was packed in a bag and kept in a dark area.

RESULTS AND DISCUSSION

Characterization and properties of self-hetero atom doped N-carbon dots

The results depicted in Figure 1(a) demonstrate the first use of pumpkin seeds as a carbon source to produce self-heteroatom doped quantum dots, and the use of "urea" as a nitrogen source has modified their surface states or passivated their edges. Once the microwave irradiation process is completed, Figure 1(b) and (c) provide a clear image of N-CDs. In the presence of sunlight, the solution appears light brown, and under UV light, it appears just as a cyan color. Our team Abdullah et al. via Springer Publishing Company previously reported on the morphology, size distribution, elemental analysis, and optical features of the as-prepared N-CDs [56]. A sizable peak at 20°–40° was seen in the X-ray diffraction pattern, which further supported the formation of tiny nanoparticles. The results also showed that, with an average size of 5-8 nm, the N-CDs exhibit a constant size distribution. The greatest peak, located at 24°, demonstrated a graphitic-like core structure with an interplaner spacing of 0.334 nm, validating the (002) lattice planning. Additionally, the various surface functional entities, such as O-H, N-H, and COO-/amide II, were identified by FTIR spectroscopy. These findings activated the surfaces of these N-CDs with oxygen-reactive species and were very helpful from an application perspective.

(a) (b) (c)

Figure 1. (a) Pumpkin seed precursor (b) Carbon dots under visible light (c) Carbon dots under UV light.

The π-π* and n-π* transitions in the N-doped CDs were linked to a large absorption zone in the wavelength range of 254-550 nm, as shown in the optical characteristics. The emission wavelength approached the red-shifted area

when the excitation wavelength was altered. The optimal emission and excitation wavelengths of the N-doped CD solution were found to be 462 and 380 nm, respectively, and it was shown to exhibit typical excitation wavelength dependence. The observed behavior of the N-doped CDs has been explained by the presence of various emissive sites on their surfaces or by differences in their diameters. Such N-doped CDs have so been proposed to have sensing capabilities. The fluorescence intensity remained steady over several hours under continuous irradiation at 380 nm, indicating their relatively strong photostability. The low direct bandgap energy of these artificial N-CDs is around 2.35 eV, or 527 nm. When compared to the reference standard quinine sulfate, distributed in 0.1 moles of H_2SO_4, the total quantum efficiency of the produced N-CDs was around 65.50%.

Composition, structural, and optical properties of TiO_2/N-CDs complex

The TiO_2/N-CDs composite material, a hybrid photocatalyst, is ready. Figure (2) illustrates the outcomes of our continued use of FTIR spectroscopy to identify surface functional groups. Let's start by discussing the composition of N-CDs. The broad peak at 3360 cm^{-1} is related to O-H and N-H stretching, while the small peak at 2950 cm^{-1} is related to CH_2 stretching. The peaks at 1642, 1537, and 1393 cm-1 are related to C=O stretching in amides, N-H deformation in amides, and OH bending in carboxylic groups. The small peaks at 1240 and 1043 are related to C-N and starching of C-O bonds, respectively. Besides, elemental composition and heteroatom doping were shown by the tiny bands at around 500 cm^{-1}.The Fourier transform infrared spectra (FTIR) of TiO_2 revealed that a large peak at 3300 cm^{-1} and 1628 cm^{-1} corresponds to O-H stretching and bending vibrations, whereas a broad band under 1000 cm^{-1} represents the distinct pure peak of TiO_2. Although the narrow band at 2930 cm^{-1} is linked with C-H and shows the surface stabilization of carbon dots onto the TiO_2 sample, the TiO_2/N-CDs composite showed all of the N-CDs peaks together with the TiO_2 main peak related with Ti-O-Ti/Ti-O-C vibrations under 1000 cm^{-1}.

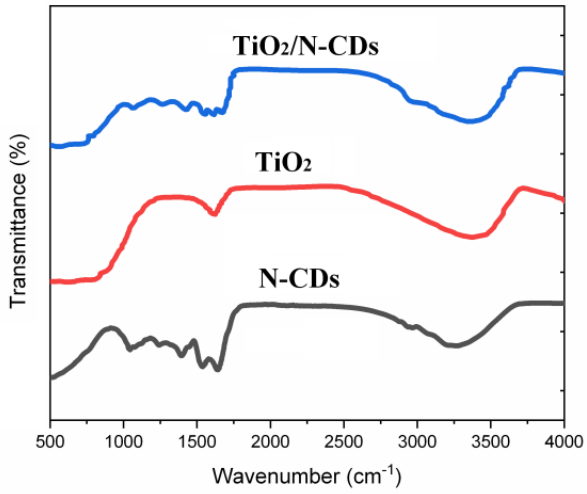

Figure 2.FTIR of N-CDs, TiO_2, and TiO_2/N-CDs nanocomposite showing different relative peaks in the complex material.

Moreover, we used CU-K(beta) radiation and an X-ray based Diffractometer to examine the crystal structural morphology of the TiO_2/N-CDs composite at a wavelength of 0.154 nm. Figure (3) illustrates the change in the TiO_2 structure following N-CD doping. The findings indicated that these N-CDs had no discernible influence on the crystal structure of TiO_2, however there was a little decrease in peaks at 25.3° and 37.8°, which are connected to the (101) and (004) planes of the anatase phase and indicated the avoidance of TiO_2 particle agglomeration. It has also been shown that the N-CDs are attached at the edge surfaces towards lateral sides by the slight rise in the peaks at 48.3°, 54.1°, 55.1°, and 62.8°, which are associated with the (200), (105),

(211), and (204) planes. In Figure 4, the entire crystal structure of the TiO_2/N-CDs nanocomposite is shown. Here, the N-CDs are affixed to the surface of the tetragonal structure of the pure anatase phase of TiO_2 material, providing a comprehensive understanding of the structure.

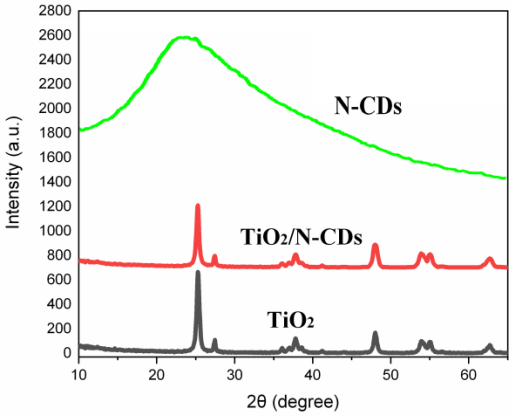

Figure 3.XRD spectroscopy of N-CDs, TiO_2 and TiO_2/N-CDs nano composite showing variation in peak intensity in TiO_2/N-CDs nanocomposite retaining its crystalline morphology but linked at the edge surface of TiO_2.

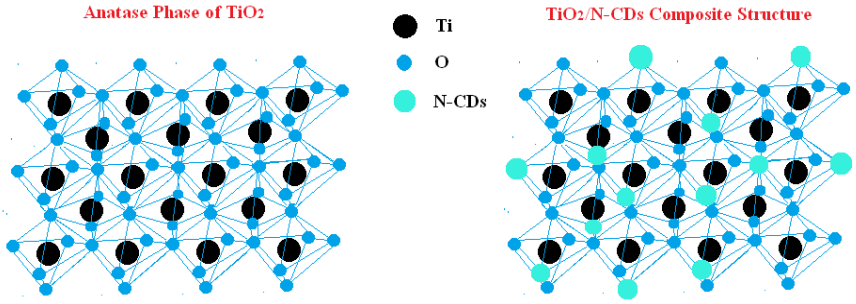

Figure 4. Tetragonal structure of anatase phase of TiO_2 and doping of N-CDs onto the surface of TiO_2 leaving basic structure unchanged.

The final results of our examination of the optical characteristics of the as-prepared TiO_2/N-CDs composite material are displayed in Figure (5). Here, we can observe that the UV spectroscopy has revealed an increase in the absorption band edge of TiO_2 from 380 to 411 nm, which is linked to a bandgaps variation from 3.26 to 3.02 eV and is primarily attributable to the excitation of newly formed Ti-O-C bonds.

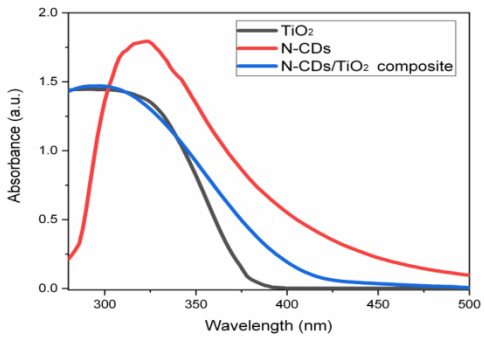

Figure 5. Figure illustrating relative absorption bands of N-CDs, TiO_2, and TiO_2/N-CDs demonstrating wide absorbing band of TiO_2/N-CDs nanocomposite towards visible light.

The effective electron mechanism within the TiO_2/N-CDs composite was examined by measuring the fluorescence of TiO_2 and TiO_2/N-CDs composite at an excitation wavelength of 290 nm. The results showed that the incorporation of N-CDs onto the TiO_2 surface resulted in the quenching of photoluminescence, indicating that effective electron transfer from N-CDs to TiO_2 occurred without photoemission. This finding can be utilized for effective photocatalysis, and the overall quenching is clearly visible in Figure 6.

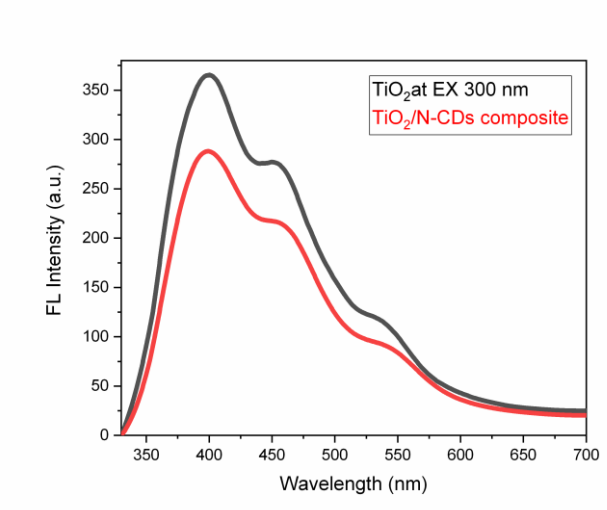

Figure 6.TiO_2/N-CDs composite showing quenching of photoluminescence due to effective electron transfer from N-CDs to TiO_2.

Electrochemical characterization

The prepared N-CDs fabricated on NF in a three-electrode cell were analyzed using cyclic voltammetry measurements, as shown in Figure 7(a). The working electrode was the N-CDs fabricated on NF in 2M of KOH at a scan rate of 10 mV/s and 20 mV/s, the counter electrode was platinum, and the reference electrode was Ag/AgCl. Figure 7(b) shows that the synthesis of N-CDs had a P-type character, with the oxidation and reduction peaks at 0.35 and 0.25 V. The p-type nature of the sample-based working electrode is also shown by a -ve slope in the Mott Schottky curve.

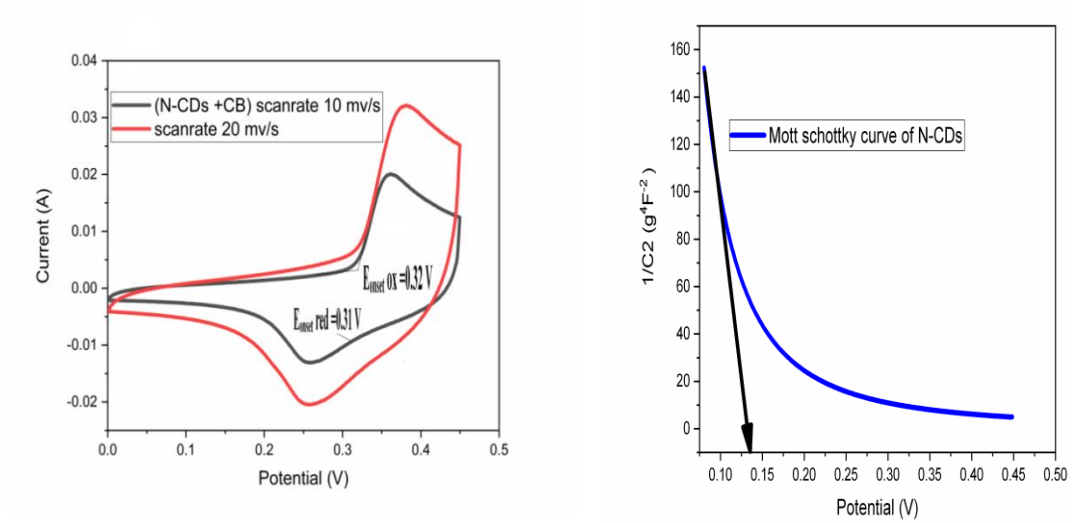

(a) (b)

Figure 7. (a) Cyclic voltammogram of N-CDs (b) Mott Schottky curve with a –ve slope indicating P-type nature of NCDs.

Given that the produced N-CDOTs have a bandgap of 2.35 eV, and the valance and conduction bands,

corresponding to these band edges, are determined using cyclic voltammetry data sets, or more specifically, by $E_{onset\ oxidation\ potential}$ and $E_{onset\ reduction\ potential}$.

The valence and conduction band edges were calculated using formulae (1 and 2), are -4.98 eV and -2.63 eV.

$$E_{CB} = -(E_{ONSET\ OX} + 4.66)eV. (1)$$

$$E_{VB} = -(E_{CB} - E_g)eV. (2)$$

Detection of Hg^{2+} ions

Evaluating the efficacy of fluorescence quenching in the presence of different ambient hazardous metal ions, such as Hg^{2+},Zn^{2+}, Pb^{2+}, Ni^{2+}, Ca^{2+}, Cu^{2+}, and Mg^{2+} allowed us to examine the N-CDs' selectivity towards Hg^{2+}. Figure 8(a) demonstrated that under identical circumstances, these representatives (metal ions) caused variations in their relative PL intensity (F/F0) of the CNDs, and the maximum photoluminescent quenching was caused by Hg^{2+} metal ion. After, the addition of more Hg^{2+} concentration to the buffer solution showed a much reduced PL quenching however, no further appreciable reduction was seen at the current concentration of these N-CDs. These findings suggested that the N-CDs have a strong affinity for Hg^{2+} detection. This is because, Hg^{2+} has a greater affinity for the carboxylic and amide groups on the surface of N-CDs, and caused the exceptional selectivity and specificity towards Hg^{2+}metal ion specimen rather than any other metal ion demonstrated above. As a result, the interaction between N-CDs and Hg^{2+} ions induced by these functional groups, resulted in the fluorescence quenching of the as-prepared N-CDs nanomaterial.

The photoluminescence spectra at various Hg^{2+} concentrations showed us the system's sensitivity, and the findings/results demonstrated that the concentration of Hg^{2+} diminished the PL spectra intensity as illustrated in Figure 8(b). The detection limit comes out to be 20-30nM, which comes under the allowed amount of mercury in drinking water by the International World Health Organisation (6 ppb, 30 nM). Furthermore, the quenching rate with concentration of $Hg^{2+}$and N-CDs demonstrated that at higher concentrations of Hg^{2+} the sensing performance is more reliable and accurate. This can be seen in Figure(9), however,98% PL was recovered by adding the iodide to the buffer solution resulting in the formation of mercurous iodide, which then removed the Hg^{2+} from the N-CDs surface, and hence PL intensity was recovered back.

Following Table 1 demonstrates the sensitivity responses of various metal ions by adding these unique novel heteroatom doped carbon dots to the buffer solutions of different metal ions.

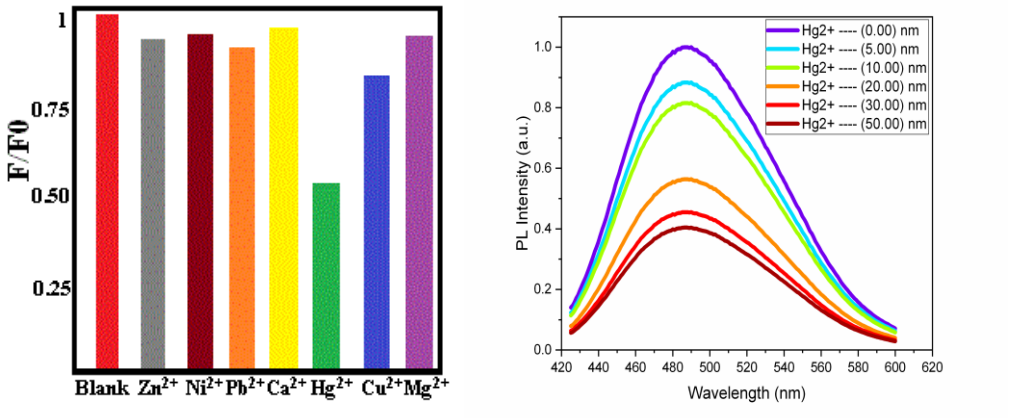

(a) (b)

Figure 8. (a) Figure showing max selectivity of Hg^{2+} by N-CDs among various metal ions (b) PL spectra of N-CDs showing the sensitivity of Hg^{2+} at different concentrations (from top to bottom: 0.00, 0.005, 0.01, 0.020, 0.030 and 0.050 μM).

Table 1. Demonstration of sensing capability of uniquely doped carbon dots.

Carbon Dots	Ion	Media/Buffer	Lower Limit(µM)	Fluorescence	Reference
Pu-erh Tea-based CDs	Cu^{2+}	-	0.051	FL intensity decreased at 435 nm	[57]
Ammonium citrate-based, N-doped CDs	Cu^{2+}	-	0.080	FL intensity decreased at 365 nm	[58]
N-S-CDs	Hg^{2+}/Fe^{3+}	-	1.40/0.160	-	[59]
N-CDs	Hg^{2+}	Phosphate	0.020	-	This work

It has been deduced that the present study gives better results than the previous studies due to the incorporation of heteroatom doping concentration of various active elements present on the surface of carbon dots.

Further, spring water and tap water from the nearby city of Kulgam in India were tested to see how well this FL sensing system worked with actual water samples. Here 5, 10, 20, 30, and 50nM's of Hg^{2+} were added to these two water samples, and the findings showed almost 98% identical results to that of the buffered pure water dispersion samples illustrated in Figure 9. Thus, N-CDs offer enormous potential for environmental pollution monitoring.

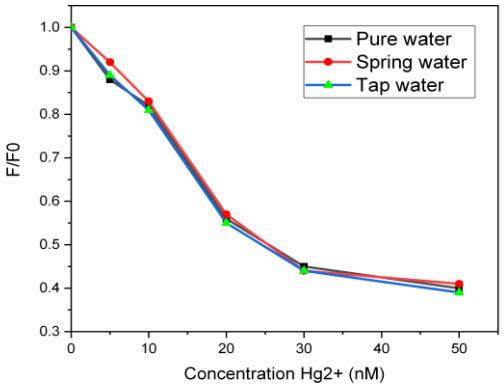

Figure 9. Photoluminescent quenching rate of N-CDs in DI, spring, and tap water against the concentration of Hg^{2+} ions.

Photocatalytic degradation of Congo red azo dye

The prepared N-CDs have high fluorescent luminescence efficiency, and multi-atom doping concentration, which makes them suitable for the photo-catalytic destruction of environmentally hazardous dyes. The combination of TiO_2 and heteroatom-doped N-CDs, or TiO_2/N-CDs, has demonstrated the better photo-catalytic performance, while using them as a photo-catalyst for the UV degradation of Congo red in this instance. To achieve the photodegradation, a complete adsorption-desorption of the dye molecules, should occur. 100 mg of hybrid photocatalyst (TiO_2/N-CDs) amalgam was combined with 250 mg/L of CR in a glass beaker and thoroughly dissolved for several minutes and later the mixture was incubated for 30 hours at room temperature and pressure conditions. These solutions were taken separately and subjected to UV (280-310) nm LED light for around 20 minutes to find the effects of UV irradiation on the degradation of the dye by this hybrid nanomaterial, also, a portion of the sample was extracted from the solution every six minutes until the dye tested, displayed a noticeable deterioration. In addition, for comparison purposes, we switched a comparable quantity of individual reference N-CDs to act as hybrid photocatalysts at the same pressure and temperature circumstances and sample measurement was taken after eighteen minutes and has clearly shown the reduction of CR to 40%, which can be visualized in UV spectroscopy plot shown in Figure 10(a), as it is clear from Figure 10(b) that the TiO_2/N-CDs nanocomposite functioned better as an effective photocatalyst than the solo N-CDs.

Therefore, we have observed an increase in the TiO_2/N-CDs nanocomposite's photocatalytic performance activity towards the degradation of CR azo dye, which is primarily attributable to the mutual collaboration of TiO_2 nanoparticles and NSP-CDs. In addition, the surfaces of heteroatom-doped N-CDs possess diverse rich edges, high-density redox-active centers, and uneven defects, as determined by the electrochemical activity of N-CDs. As a result of these characteristics, the overall catalytic activity has been increased which efficiently transferred photoexcited electrons from TiO_2 to N-CDs, which ultimately reduces the electron and hole recombination and boosts efficiency.

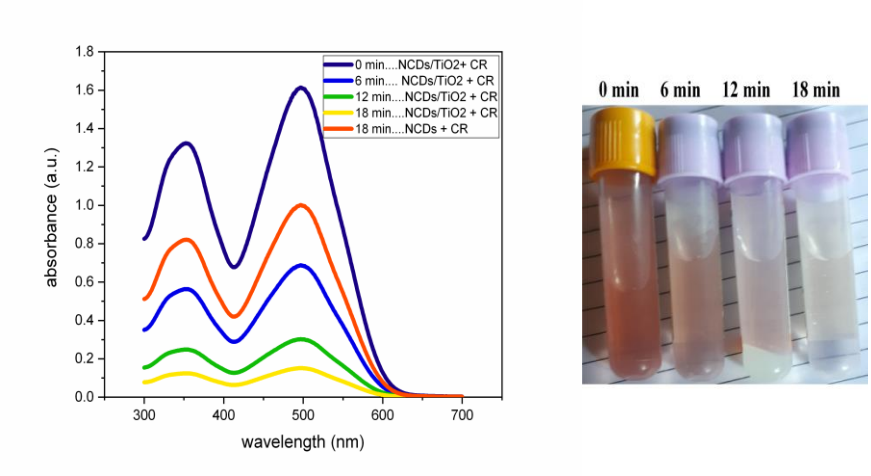

(a) (b)

Figure 10.(a) UV abs spectrum of CR against irradiation time in the presence of N-CDs and hybrid photocatalyst TiO_2/N-CDs (b) Photodegradation of real-time CR dye at various irradiation time intervals.

The kinetics of photo-degradation and reaction degradation is depicted in Figure 11(a, b), which effectively displays the pseudo-first-order kinetics calculated by equation (3):-

$$\ln(C/C_0) = kt \quad (3)$$

Where t(min) is the irradiation period and k(min^{-1}) is the rate constant. As contrast to the innovative hybrid N-CDs/TiO_2 nanocomposite, which demonstrated a maximum attainable value of k_2 = 0.1323min-1, the degradation reaction rate constants, k_1 and k_2, clearly indicated that pure N-CDs employed as solo reference photocatalyst has a low rate constant, k_1 = (0.027min-1). The research findings indicate that the newly developed hybrid N-CDs/TiO_2nanocomposite shown exceptional photocatalytic activity.

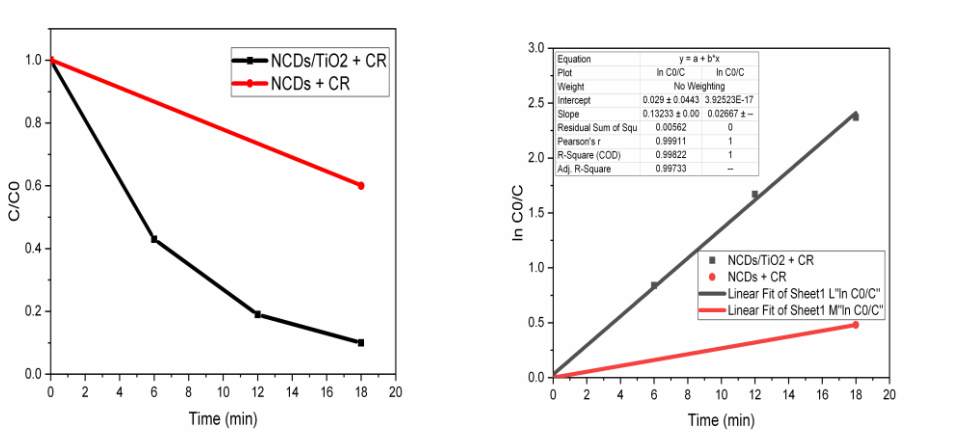

(a) (b)

Figure 11. (a) Photo-degradation of Congo red dye with N-CDs and N-CDs/ TiO_2 (b) Visualization of Photo-degradation kinematics demonstrated the first order kinetics with high rate constant.

There was a built-in electric field E from TiO_2 towards the N-CDs and a p-n junction formed as the P-type N-CDs were deposited onto the n-type TiO_2 edges. This was caused by the electrons, diffusing from the N-CDs side to the TiO_2 side due to the difference in Fermi energies. Short UV light was used to activate the N-CDs/TiO_2 hybrid photoanode.Due to the intrinsic electric field, which lowers the energy level difference between N-CDs and TiO_2, the photogenerated electrons in the N-CDs' conduction band moved towards the conduction band of TiO_2. Meanwhile, the holes accumulated on TiO_2's valance band continued to migrate towards the N-CDs' valance band, inhibiting the direct recombination of the photogenerated electron-hole pairs. Pollutant degradation was accelerated by the efficient and quick transfer of the photogenerated carriers by the electric field, which left the free charge carriers fully engaged in the generation of ROS species. It is well known that photogenerated electrons on the CB can make $\cdot O2^-$ superoxide species, and the photogenerated holes on the VB may oxidize water to produce $\cdot OH^-$ radicals. As seen in Figure 12, these two radicals are essential for the breakdown of dye molecules into CO_2 and H_2O, the ultimate products of the dye molecule disintegration. Therefore, the N-CDs/TiO_2 hybrid performs well in the degradation of dangerous dyes that are commonly found in our surroundings.

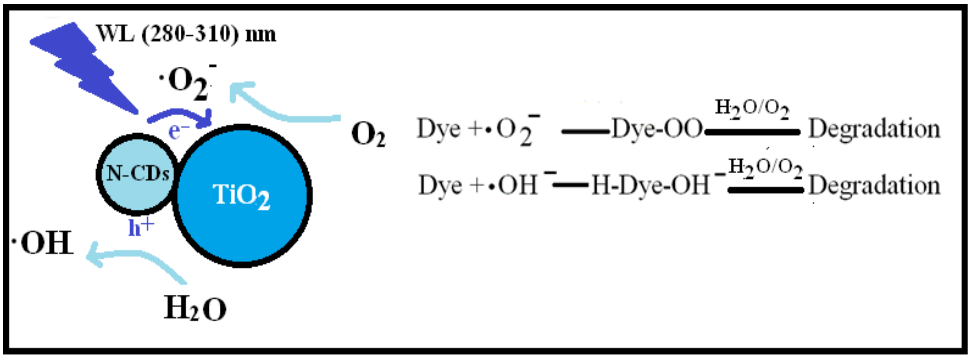

Figure 12. Graphical illustration of the mechanism of degradation of azo Dyes.

The following Table (2), represents the degradation efficiencies of different organic dyes by N-CD-based TiO_2photocatalyst and the results have demonstrated greater degradation efficiency of this N-CDs/TiO_2nanocomposite in a very much lesser time against previous studies.

Table 2. Table showing previous studies of TiO_2/N-CDs against degradation of various dyes.

Catalyst/Dye	Light/Rate constant	Time(min)/Degradation %	Reference
NCQDS/TNSs@Cu_2O/MO/CR	Visible/ 0.106	60/99	[60]
N-GQDs/TiO_2/MB	UV (410 nm)/-	17/85	[61]
CQDs-x/TiO_2/Organic compound	Visible/-	40-60/50-70	[62]
CQDs/TiO_2/CR	UV/-	30/64.72	[63]
CQDs/TiO_2/Rh-B	Visible	30/85.47	[64]
N-CDs/TiO_2/CR	UV/0.1068	18/90	This work
N-CDs/CR	UV/0.020	18/40	This work

CONCLUSIONS

Here we have explored our previously synthesized Heteroatom-doped N-carbon dots synthesized from easily available pumpkin seeds. They have demonstrated a high FL quantum yield of 65.50% associated with a lower energy gap of 2.35 eV. Here, we have efficiently, utilized these N-CDs towards the sensitive and selective detection of the Hg^{2+} metal ions among various other metal ions and the LOD comes out to be 20-30 nM's, mainly due to the interaction of various surface functional groups through coordination bonds, electrostatic interactions and chemical reactions which have altered the optical property of N-CDs leading to

measurable change in fluorescence intensity and therefore, can be used for enhancing the water quality checks for commercial use. Moreover, the N-CDs significantly increased TiO_2's photocatalytic activity under UV (280-310) nm illumination by breaking down 90% of the toxic Congo red azo dye in just 18 minutes of irradiation time. This is in contrast with the reference solo N-CDs photo-catalysts performance, which has achieved 40% of degradation efficiency. The achieved photodegradation was mainly due to the formation of ROS in the water solvent system thereby, forming multiple active sites and defects in the composite, ultimately led to the phenomena of adsorption and reduction of oxygen species from the dye molecules, under UV light irradiation and hence, prevented the recombination of electrons and holes within the composite, resulting effective electron transport from N-CDs to TiO_2 and vice versa, or physically absorb dye molecules, resulting a good measurable photocatalytic degradation of toxic dyes. Therefore, these new N-CD/TiO_2nanohybrids could be a better choice for tracking and get rid of environmental contaminants.

ACKNOWLEDGEMENTS

I would like to extend my gratitude to Govt Degree College for Women Anantnag, NIT Srinagar and Bhagwant University, Ajmer for their support in providing resources, infrastructure and immeasurable moral support in this endeavor.

I wish to dedicate this research work paper to my parents Bashir Ahmad and Dilshada Banu and my brothers and sisters especially my wife and daughter Yasmeena and Aisha Abdullah who have always been an endless source of inspiration and joy in my life.

Conflict of interests

There are no conflicts of interest to declare by the authors.

Funding statement

No overall funding for this work.

Data availability

The datasets generated during and/or analysed during the current study are available from the corresponding author on reasonable request.

Supplementary information:

Not applicable.

REFERENCES

1. Xu X.Y., Ray R., Gu Y.L., Ploehn H.J., Gearheart L., Raker K., Scrivens W.A., 2004. Electrophoretic analysis and purification of fluorescent single-walled carbon nanotube fragments. Journal of American Chemical Society. 126(40), 12736–12737.

2. Sun Y.P., Bing Z., Yi L., Wei W., Fernando K.A.S., Pathak P., Meziani M.J., Harruff B.A., Xin W., Wang H., 2006. Quantum-sized carbon dots for bright and colorful photoluminescence. Journal of American Chemical Society. 128(24), 7756–7757.

3. Zhang M.R., Su R., Zhong J., Fei L., Cai W., Guan Q.W., Li W.J., Li N., Chen Y.S. Cai L.L., 2019. Red/orange
dual-emissive carbon dots for pH sensing and cell imaging. Nano Research. 12, 815–821.

4. Zhang Y.N., Zhang X.W., Shi Y.P., Sun C., Zhou N., Wen H.X., 2020. The synthesis and functional study of multicolor nitrogen-doped carbon dots for live cell nuclear imaging. Molecules. 25(2), 306.

5. Liu J.J., Dong Y.Y., Ma Y.X., Han Y.X., Ma S., Chen H.L., Chen X.G., 2018. One-step synthesis of red/green dual-emissive carbon dots for ratiometric sensitive $ONOO^-$ probing and cell imaging. Nanoscale. 10, 13589–13598.

6. Qin K.H., Zhang D.F., Ding Y.F., Zheng X.D., Xiang Y.Y., Hua J.H., Zhang Q., Ji X.L., Li B., Wei Y.L., 2020. Applications of hydrothermal synthesis of Escherichia coli derived carbon dots in in-vitro and in-vivo imaging and p-nitrophenol detection. Analyst. 145, 177–183.

7. Liu J.J., Li D.W., Zhang K., Yang M.X., Sun H.C., Yang B., 2018. One step hydrothermal synthesis of nitrogen-doped conjugated carbonized polymer dots with 31% efficient red emission for In-Vivo imaging. Small. 14(15), 1703919–1703929.

8. Shu Y., Lu J., Mao Q.X., Song R.S., Wang X.Y., Chen X.W., Wang J.H., 2017. Ionic liquid mediated

organophiliccarbon dots for drug delivery and bioimaging. Carbon. 114, 324–333.

9. Kailasa S.K., Bhamore J.R., Koduru J.R., Park T.J., 2019. Carbon dots as carriers for the development of controlleddrug and gene delivery systems. Biomedical Applications of Nanoparticles. Chapter 11. pp. 295–317.

10. Yang T., Huang J.L., Wang Y.T., Zheng A.Q., Shu Y., Wang J.H., 2019. β-cyclodextrin-decorated carbon dots serveas nanocarriers for targeted drug delivery and controlled release. Chem Nano Mat. 5(4), 479–487.

11. Jana J., Lee H.J., Chung J.S., Kim M.H., Hur S.H., 2019. Blue emitting nitrogen-doped carbon dots as a fluorescentprobe for nitrite ion sensing and cell-imaging. Analytica Chimica Acta. 1079, 212–219.

12. Wang J., Li R.S., Zhang H.Z., Wang N., Zhang Z., Huang C.Z., 2017. Highly fluorescent carbon dots as selective and visual probes for sensing copper ions in living cells via an electron transfer process. Biosensors and Bioelectronics. 97, 157–163.

13. Hu J., Tang F., Jiang Y., Liu C., 2020. Rapid screening and quantitative detection of Salmonella using a quantum dot nanobead-based biosensor. Analyst. 145(6), 2184–2190.

14. Han M., Zhu S.J., Lu S., Song Y.B., Feng T.L., Tao S.Y., Liu J.J., Yang B., 2018. Recent progress on the photocatalysis of carbon dots: Classification, mechanism and applications. Nano Today. 19, 201–218.

15. Yu H.J., Shi R., Zhao Y.F., Waterhouse G.I., Wu L.Z., Tung C.H., Zhang T.R., 2016. Smart utilization of carbondots in semiconductor photocatalysis. Advanced Materials. 28(43), 9454–9477.

16. Zhou Y., Zahran E.M., Quiroga B.A., Perez J., Mintz K.J., Peng Z., Liyanage P.Y., Pandey R.R., Chusuei C.C., Leblanc R.M., 2019. Size-dependent photocatalytic activity of carbon dots with surface-state determined photoluminescence. Applied Catalysis B: Environmental. 248, 157–166.

17. Yuan F.L., Yuan T., Sui L.Z., Wang Z.B., Xi Z., Li Y.C., Li X.H., Fan L.Z., Tan Z.A., Chen A et al., 2018. Engineering triangular carbon quantum dots with unprecedented narrow bandwidth emission for multicolored LEDs. Nature Communications. 9, 2249–2260.

18. Zheng J.X., Liu X.H., Yang Y.Z., Liu X.G., Xu B.S., 2018. Rapid and green synthesis of fluorescent carbon dots from starch for white light-emitting diodes. New Carbon Materials. 33(3), 276–288.

19. Hu C., Li M.Y., Qiu J.S., Sun Y.P., 2019. Design and fabrication of carbon dots for energy conversion and storage. Chemical Society Reviews. 48(8), 2315–2337.

20. Fernando K.S., Sahu S., Liu Y., Lewis W.K., Guliants E.A., Jafariyan A., Wang P., Bunker C.E., Sun Y.P., 2015Carbon quantum dots and applications in photocatalytic energy conversion. ACS Applied Material & Interfaces. 7(16), 8363–8376.

21. Genc R., Alas M.O., Harputlu E., Repp S., Kremer N., Castellano M., Colak S.G., Ocakoglu K., Erdem E., 2012. High-capacitance hybrid supercapacitor based on multi-colored fluorescent carbon-dots. Scientific Reports. 7, 11222.

22. Zhu C., Zhai J., Dong S., 2012. Bifunctional fluorescent carbon nanodots: green synthesis via soy milk and application as metal-free electrocatalysts for oxygen reduction. Chemical communications. 48(75), 9367-9369.

23. Huang H., Lv J.J., Zhou D.L., Bao N., Xu Y., Wang A.J., Feng J.J., 2013. One-pot green synthesis of nitrogen doped carbon nanoparticles as fluorescent probes for mercury ions. RSC Advances. 3(44), 21691–21696.

24. M Xue., M Zou., J Zhao., Z Zhan., S Zhao., 2015. Green preparation of fluorescent carbon dots from lychee seeds and their application for the selective detection of methylene blue and imaging in living cells. Journal of Materials Chemistry B. 3(33), 6783–6789.

25. Wang D., Wang X., Guo Y., Liu W., Qin W., 2015. Imidazole derivative-functionalized carbon dots: using as a fluorescent probe for detecting water and imaging of live cells. Dalton Transactions. 44(12), 5547–5554.

26. Yu D., Nagelli E., Du F., Dai L., Phys J., 2010. Metal-free carbon nanomaterials become more active than metal catalysts and last longer. The Journal of Physical Chemistry Letters. 1(14), 2165–2173.

27. Bindra P., Hazra A., 2018. Capacitive gas and vapor sensors using nanomaterials. Journal of Materials Science: Materials in Electronics. 29(8), 6129–6148.

28. Renzoni A., Zino F., Franchi E., 1998. Mercury Levels along the Food Chain and Risk for Exposed Populations. Environmental Research. 77(2), 68-72.

29. Driscoll T., MasonP., ChanM., JacobJ., PirroneN., 2013, May 21. Mercury as a Global Pollutant: Sources,

Pathways, and Effects. Environmental Science and Technology. 47(10), 4967–4983.

30. Liu J., Lu Y., 2007. Rational design of "turn-on" allosteric DNAzyme catalytic beacons for aqueous mercury ions with ultrahigh sensitivity and selectivity. Angewandte Chemie International Edition. 46(40), 7587-7590.

31. Gutknecht J., 1981. Inorganic mercury (Hg^{2+}) transport through lipid bilayer membranes. The Journal of Membrane Biology. 61, 61–66.

32. K Leopold, M Foulkes, P Worsfold., 2010. Methods for the determination and speciation of mercury in natural waters-A review. Analytica chimica acta. 663(2), 127-138.

33. Gong Y.J, Zhang X.B, Zhang C.C, Luo A.L, Fu T, Tan W, Shen G.L, Yu R.Q., 2012. Through Bond Energy Transfer: A Convenient and Universal Strategy toward Efficient Ratiometric Fluorescent Probe for Bioimaging Applications. Analytical Chemistry. 84(24), 10777–10784.

34. Lin Y.H., Tseng W.L., 2010. Ultrasensitive sensing of $Hg(^{2+})$ and $CH(_3)Hg(^{+})$ based on the fluorescence quenching of lysozyme type VI-stabilized gold nanoclusters. Analytical Chemistry. 82(22), 9194-9200.

35. Chong M.N., Jin B., Chow C.W.K., Saint C., 2010. Recent developments in photocatalytic water treatment technology: A review. Water Research. 44 (10) 2997–3027.

36. A Kubacka., M. Fernandez Garcia., G Colon., 2012. Advanced nanoarchitectures for solar photocatalytic applications. Chemical Reviews. 112 (3), 1555–1614.

37. R Atchudan., T.N Jebakumar Immanuel Edison., S Perumal., Karthikeyan D., Lee Y.R., 2017. Effective photocatalytic degradation of anthropogenic dyes using graphene oxide grafting titanium dioxide nanoparticles under UV-light irradiation. Journal of Photochemistry and Photobiology A: Chemistry. 333, 92–104.

38. Wang J.L., Xu L.E., 2012. Advanced Oxidation Processes for Wastewater Treatment: Formation of Hydroxyl Radical and Application. Critical Reviews in Environmental Science and Technology. 42(3), 251-325.

39. Safardoust Hojaghan H., Salavati Niasari M., 2017. Degradation of methylene blue as a pollutant with N-doped graphene quantum dot/titanium dioxide nanocomposite. Journal of Cleaner Production. 148, 31–36.

40. Mohd Abdullah Sh., Khan A., Chandok R S., 2022. A Compressive study on Biomass derived Carbon dots. Asian Journal of Organic and Medicinal Chemistry. 7(2), April-June Special Issue-II, 568-605.

41. Prawit N., Chanthai S., Mahachai R., Oh W.C., 2016. Sonocatalytic performance of ZnO /graphene/ TiO_2nanocomposite for degradation of dye pollutants (methylene blue, texbrite BAC-L, texbrite BBU-L and texbrite NFW-L) under ultrasonic irradiation. Dyes and Pigments. 134, 487–497.

42. Atchudan R., Thomas N.J.I Edison., Perumal S., Vinodh R., Lee Y.R., 2018. In-situ green synthesis of nitrogen-doped carbon dots for bioimaging and TiO_2 nanoparticles@ nitrogen-doped carbon composite for photocatalytic degradation of organic pollutants. Journal of Alloys and Compounds. 766, 12–24.

43. Zhao D., Sheng G., Chen C., Wang X., 2012. Enhanced photocatalytic degradation of methylene blue under visible irradiation on graphene@TiO_2 dyade structure. Applied Catalysis B: Environmental. 111-112, 303–308.

44. Wu F., Li X., Liu W., Zhang S., 2017. Highly enhanced photocatalytic degradation of methylene blue over the indirect all-solid-state Z-scheme g-C_3N_4-RGO-TiO_2 nano-heterojunctions. Applied Surface Science. 405, 60–70.

45. Chen J., Shu J., Anqi Z., Juyuan H., Yan Z., Chen J., 2016. Synthesis of carbon quantum dots/TiO_2 nanocomposite for photo-degradation of Rhodamine B and cefradine. Diamond and Related Materials. 70, 137–144.

46. Hasan M.T., Gonzalez Rodriguez R., Ryan C., Faerber N., Coffer J.L., Naumov A.V., 2018. Photo-and electroluminescence from nitrogen-doped and nitrogen–sulfur codoped graphene quantum dots. Advanced Functional Materials. 28(42), 1804337.

47. Jiqian Y., Xianlong Z., Dihua W., Xudong Z., Zhen Z., 2017. S-doped N-rich carbon nanosheets with expanded interlayer distance as anode materials for sodium-ion batteries. Advanced Materials. 29(6), 1604108.

48. Sheikh M.A., Chandok R.S., Abida Khan., 2024. Green perspective of N-CDs towards energy crisis and

photodegradation of toxic dyes. Discover Materials. 4(1), 9.

49. Mohd Abdullah Sh., Khan A., Chandok R.S., 2022. Oxide Based Nano-Sensors For Industrial And Environmental Monitoring. Journal of Optoelectronics Laser. 41(5), 907–927.

50. Sheikh M.A., Chandok R.S., Abida K., 2024. Revolutionizing the sensing properties of green carbon dots for monitoring carbon dioxide and carbon monoxide at room temperature. Carbon Letters. Online first.

51. El Amri A., Kadiri L., Hsissou R., Lebkiri A., Wardighi Z., Rifi E., Lebkiri A., 2023. Investigation of Typha Latifolia (TL) as potential biosorbent for removal of the methyl orange anionic dye in the aqueous solution: Kinetic and DFT approaches. Journal of Molecular Structure. 1272, 134098.

52. Jaouad B., Abdennacer I., El Faydy M., Doumane Gh., Staoui A., Hsissou R., Lebkiri A., Habsaoui A., Zarrouk A., El Housseine R., 2023. Investigation of the cationic resin as a potential adsorbent to remove MR and CV dyes: Kinetic, equilibrium isotherms studies and DFT calculations. Journal of Molecular Structure. 1278(5), 134849.

53. Assia J., Abdelhay., Rachid H., Azzedine L., Basma Z., Fatima Z.B., El mahdi H., El Housseine R., Ahmed L., 2023. Synthesis of a chitosan@hydroxyapatite composite hybrid using a new approach for high-performance removal of crystal violet dye in aqueous solution, equilibrium isotherms and process optimization. Journal of the Taiwan Institute of Chemical Engineers. 149,105006.

54. Imane L., Brahim A., Rachid H., Zaki S., Makfire S., Avni B., Abdelhay E., Essaadaoui Y., Lamya K., Ahmed L., El Rifi H., 2023. Investigation of the anionic polyacrylamide as a potential adsorbent of crystal violet dye from aqueous solution: Equilibrium, kinetic, thermodynamic, DFT, MC and MD approaches. Journal of Molecular Liquids. 372(17), 121220.

55. Kadiri L., Ouass A., Hsissou R., Safi Z., Wazzan N., Essaadaoui Y., Lebkiri I., El Khattabi O., Rifi E., Lebkiri A., 2021. Adsorption properties of coriander seeds: Spectroscopic kinetic thermodynamic and computational approaches. Journal of Molecular Liquids. 343(11), 116971.

56. Sheikh M.A., Chandok R.S., Abida K., 2023. High energy density storage, antifungal activity and enhanced bioimaging by green self-doped heteroatom carbon dots. Discover Nano. 18(1), 132.

57. Zhang W., Li N., Chang Q., Chen Z., Hu S., 2020. Making a Cup of Carbon Dots for Ratiometric and Colorimetric Fluorescent Detection of Cu^{2+} Ions. Colloids and Surfaces A.: Physicochemical and Engineering Aspects. 586, 124233.

58. Sun Y., Wei M., Liu R., Wang H., Li H., Kang Q., Shen D., 2019. A Smartphone-Based Ratiometric Fluorescent Device for Field Analysis of Soluble Copper in River Water Using Carbon Quantum Dots as Luminophore. Talanta. 194, 452–460.

59. Liu H., Xu H., Li H., 2022. Detection of Fe^{3+} and Hg^{2+} Ions by Using High Fluorescent Carbon Dots Doped With S And N as Fluorescence Probes. Journal of Fluorescence. 32(3), 1089–1098.

60. Huihui F., Zhang Y., Cui F., 2022. Enhanced photocatalytic activity of Cu_2O for visible light-driven dye degradation by carbon quantum dots. Environmental Science and Pollution Research. 29(7), 8613-8622.

61. Safardoust-Hojaghan H., Salavati-Niasari M., 2017. Degradation of methylene blue as a pollutant with N-doped graphene quantum dot/titanium dioxide nanocomposite. Journal of Cleaner Production. 148, 31–36.

62. Hu X., Han W., Zhang M., Li D., Sun H 2022. Enhanced adsorption and visible-light photocatalysis on TiO_2 with in situ formed carbon quantum dots. Journal of Environmental Science and Pollution Research. 29(37), 56379–56392.

63. Sathish Kumar M., Yashoda K.Y., Kumaresan D., Nikhil K K., Sudip K B., 2018. TiO_2-carbon quantum dots (CQD) nanohybrid: enhanced photocatalytic activity. Materials Research Express. 5(7), 075502.

64. Harun N.H., Rahman M.N.A., Kamarudin W.F.W., Irwan Z., Muhammud A., Akhir N.E.F.M., Yaafar M.R.,2018. Photocatalytic Degradation Of Congo Red Dye Based On Titanium Dioxide Using Solar And UV Lamp. Journal of Fundamental and Applied Sciences. 20168, 10(1S), 832-846.